Short- and Long-term Forms of Neural Adaptation: An ERP Investigation of Dynamic Motion Aftereffects

Sibel Akyuz[1, 2, 3], Andrea Pavan[4], Utku Kaya[2, 5], Hulusi Kafaligonul[1, 2*]

[1]Interdisciplinary Neuroscience Program, Bilkent University, Ankara, Turkey

[2]National Magnetic Resonance Research Center (UMRAM), Bilkent University, Ankara, Turkey

[3]Faculty of Arts and Sciences, Osmaniye Korkut Ata University, Osmaniye, Turkey

[4]School of Psychology, University of Lincoln, Brayford Wharf East, Lincoln LN5 7AY, UK

[5]Department of Anesthesiology, University of Michigan, Ann Arbor, MI

[*]Correspondence:

Hulusi Kafaligonul

Aysel Sabuncu Brain Research Center

Bilkent University, Ankara, Turkey 06800

Email: hulusi@bilkent.edu.tr

Phone: +90 312 290 3016

ABSTRACT

Adaptation is essential to interact with a dynamic and changing environment, and can be observed on different timescales. Previous studies on a motion paradigm called dynamic motion aftereffect (dMAE) showed that neural adaptation can establish even in very short timescales. However, the neural mechanisms underlying such rapid form of neural plasticity is still debated. In the present study, short- and long-term forms of neural plasticity were investigated using dynamic motion aftereffect combined with EEG (Electroencephalogram). Participants were adapted to directional drifting gratings for either short (640 ms) or long (6.4 s) durations. Both adaptation durations led to motion aftereffects on the perceived direction of a dynamic and directionally ambiguous test pattern, but the long adaptation produced stronger dMAE. In line with behavioral results, we found robust changes in the event-related potentials elicited by the dynamic test pattern within 64-112 ms time range. These changes were mainly clustered over occipital and parieto-occipital scalp sites. Within this time range, the aftereffects induced by long adaptation were stronger than those by short adaptation. Moreover, the aftereffects by each adaptation duration were in the opposite direction. Overall, these EEG findings suggest that dMAEs reflect changes in cortical areas mediating low- and mid-level visual motion processing. They further provide evidence that short- and long-term forms of motion adaptation lead to distinct changes in neural activity, and hence support the view that adaptation is an active time-dependent process which involves different neural mechanisms.

Keywords: neural adaptation, dynamic motion aftereffect, short-term, long-term, event-related potentials

1. Introduction

Human perception is shaped by the actual pattern of sensory inputs and previous experience with the external world. Phenomena such as motion adaptation have been extensively employed to understand how previous sensory experience, usually operating over different timescales, contribute to perception (Clifford, 2002; Kohn, 2007; Krekelberg, Boynton, & Van Wezel, 2006). After a prolonged exposure (i.e., tens-hundreds of seconds) to an object moving in a particular direction and with a certain speed, a subsequent motion percept in the opposite direction is produced. This illusion is known as motion aftereffect (MAE), and has been considered to be a phenomenon deemed worthy of study in its own right but also a powerful tool for investigating mechanisms underlying different forms of neural plasticity and their functional roles in perception (see Mather, Pavan, Campana, & Casco, 2008 for a review).

To understand the neural substrates underlying MAE, different types of adapter and test patterns engaging distinct stages of motion processing have been frequently used. This led to variants of experimental paradigms based on MAE illusion. An interesting type is called dynamic motion aftereffect (dMAE), in which a dynamic test pattern (i.e., a counterphase flickering pattern with no net motion direction) is used. Although such dynamic test pattern simultaneously activates early motion detectors sensitive to opposite directions, it is also typically perceived as directional which is determined at higher levels of sensory processing. Some of the previous research highlighted that dMAE has different characteristics than the classical demonstration of the illusion including only static test patterns. For instance, it is sensitive to second-order motion and can be generated by attention-based position tracking of adapting stimulus (Culham, Verstraten, Ashida, & Cavanagh, 2000; Nishida & Sato, 1995). Therefore, these findings suggest that dMAE may reflect changes in later stages of motion processing. On the other hand, other findings did not fully support this view. Kanai and Verstraten (2005) found that even brief exposure to motion (e.g., tens of milliseconds) can induce dMAE, biasing the perceived direction of a subsequently presented counterphase flickering test pattern. Behavioral studies on this rapid form of dMAE have suggested that it can tap low- and mid-levels of motion processing (Pavan, Campana, Guerreschi, Manassi, & Casco, 2009; Pavan, Campana, Maniglia, & Casco, 2010; Pavan & Skujevskis, 2013). A transcranial magnetic stimulation (TMS) study using this paradigm further indicated the involvement of both V2/V3 and V5/MT (middle temporal area) activities in dMAE

(Campana, Pavan, Maniglia, & Casco, 2011; see also Campana, Maniglia, & Pavan, 2013). Compared to area V5/MT, these TMS findings also pointed out a greater and causal involvement of V2/V3, suggesting that early visual areas play a critical role in rapid forms of dMAE.

Although previous research indicates specific neural substrates for dMAE, the neural mechanisms underlying dMAE induced changes are still debated. In particular, the neural correlates of rapid forms of dMAE and the induced neural plasticity have been scarcely investigated, and the resulting framework is fragmentary. In the present study, we focused on characterizing the timing and spatial (i.e., scalp) distribution of the dMAE induced changes in event-related potentials (ERPs). We acquired Electroencephalogram (EEG) while participants performed a motion direction discrimination task under different dMAE conditions. Critically, our approach included both sub-second (short-term) and supra-second (long-term) adaptation durations. We had two specific goals in having such experimental design. First, the exposure time to the adapter has been shown an important parameter for induced aftereffects in general (Krekelberg et al., 2006). Previous research also indicated that an increase in adaptation duration leads to stronger and more robust dMAE (Kanai & Verstraten, 2005; Oluk, Pavan, & Kafaligonul, 2016). Therefore, we aimed at identifying scalp sites and ERP components over which dMAE takes place by using adaptation duration as a critical experimental factor. Second, the adaptation induced changes in the neural responses can be observed on many timescales even in the same cortical area and neural circuit. For example, the aftereffects on V5/MT neuronal activities have been described in the sub-second time range, seconds and even in minutes (Glasser, Tsui, Pack, & Tadin, 2011; Kohn & Movhson, 2003; Krekelberg et al., 2006; Priebe, Churchland, & Lisberger, 2002; Priebe & Lisberger, 2002). These changes have been proposed to rely on different mechanisms of neural plasticity. The duration of both adapter and test stimuli have been frequently manipulated to reveal those mechanisms. Comparing the short-term aftereffects on identified ERP components with those of long-term adaptations, we wanted to determine whether the short- and long-term forms of dMAE rely on different mechanisms even over the same scalp site. If so, we expected to find distinct changes in the neural activity for sub- and supra-second adaptation durations.

2. Methods

In this section, we report how we determined our sample size, all data exclusions, all inclusion/exclusion criteria, whether inclusion/exclusion criteria were established prior to data analysis, all manipulations, and all measures in the study. No part of the study procedures or analyses was pre-registered in a time-stamped, institutional registry prior to the research being conducted.

2.1. Participants

We tested 22 adult human volunteers. All participants had normal or corrected-to-normal visual acuity and no history of neurological disorders. Prior to their participation, they were informed about experimental procedures and signed a consent form. The behavioral data of 2 participants did not meet our criteria in practice sessions (see *Stimuli and procedure*) and 1 participant had excessive EEG artifacts. Accordingly, the data of 19 participants were used in the analyses (10 females, age range 18-33 years). The sample size was estimated based on Kobayashi, Yoshino, Ogasawara and Nomura (2002) using the G*Power software in order to get a large effect size (Faul, Erdfelder, Buchner, & Lang, 2002) and it was commensurate with previous EEG studies (e.g., Kaya & Kafaligonul, 2019). The inclusion/exclusion criteria were established prior to data analysis. All procedures were in accordance with the Declaration of Helsinki (World Medical Association, 2013) and approved by the local Ethics Committee of Bilkent University and the University of Lincoln.

2.2. Apparatus

Visual stimuli were generated using Matlab 7.12 (The MathWorks, Natick, MA) with PsychToolbox 3.0 (Brainard, 1997; Pelli, 1997). They were displayed on a 20-inch CRT monitor (Mitsubishi Diamond Pro 2070sb, 1280 × 1024 pixel resolution and 100 Hz refresh rate) at a viewing distance of 57 cm. A SpectroCAL (Cambridge Research Systems, Rochester, Kent, UK) photometer was used for the luminance calibration and the linearization of the display. The minimum and maximum luminance values of the screen were 0.48 and 106.56 cd/m^2, respectively. The mean luminance was 53.52 cd/m^2. Precise temporal overlapping of triggers and the onset times of each stimulus during a trial were verified with a digital oscilloscope (Rigol DS

10204B, GmbH, Puchheim, Germany) connected to a photodiode which detected visual stimulus onsets and offsets. All data were collected in a silent and dimly lit room.

2.3. Stimuli and procedure

A white fixation point (0.3 deg diameter) was presented at the center of the screen. In order to aid fixation, the fixation point was surrounded by an annulus of 1 deg diameter at mean luminance. Adapting and test stimuli were vertically oriented Gabor patches presented at the center of the screen (Fig. 1). Gabors consisted of sinusoidal luminance modulation enveloped by a static Gaussian. They had a size of approximately 8 deg (σ = 2.22 deg), and a spatial frequency of 1 c/deg. The Michelson contrast of Gabor patches was constant at 0.9.

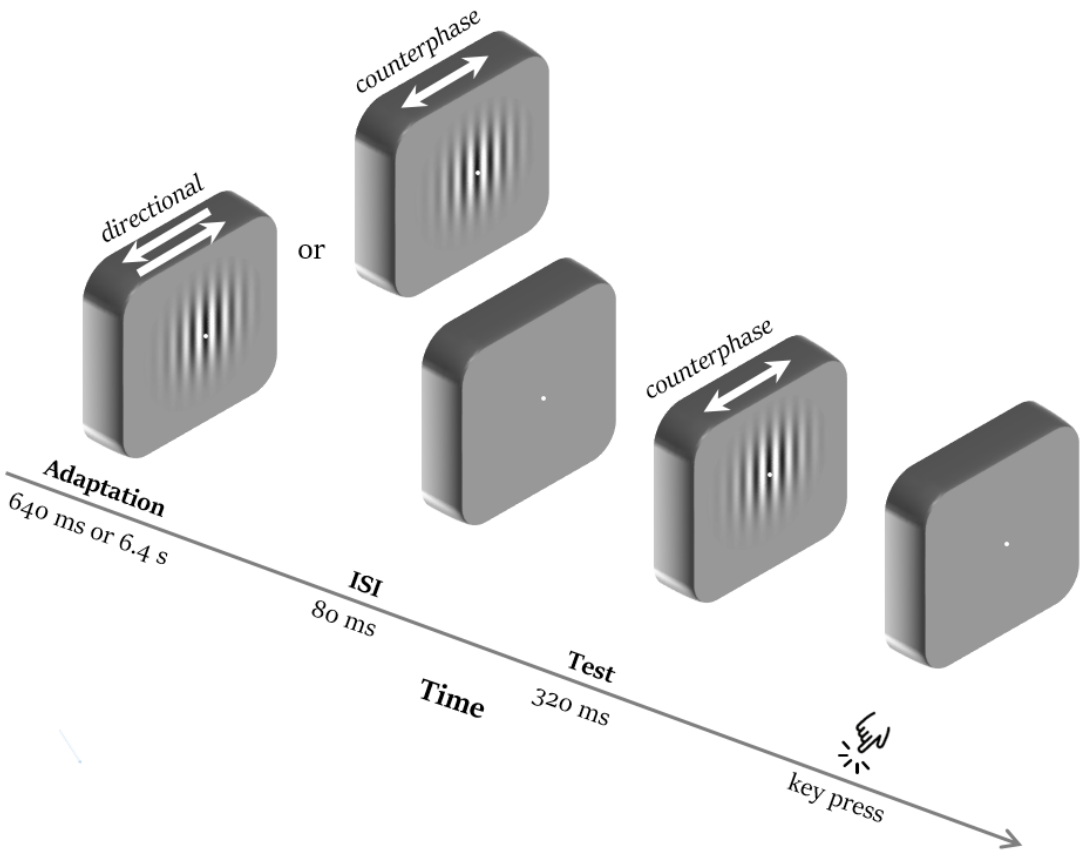

Fig. 1. Schematic representation of the stimuli and timeline. In each trial, the adapting stimulus was shown first. The adapting pattern was either counterphase flickering or directional (leftward or rightward) and its duration (short: 640 ms or long: 6.4 s) was varied across trials. After an 80 ms adapting-test blank interval, the counterphase flickering test pattern was displayed for 320 ms.

Adapting Gabor patches could be either drifting in one direction (leftward or rightward) or counterphase flickering (i.e., directionally ambiguous), whereas test stimuli were always counterphase flickering patches. A temporal frequency of 6.25 Hz was used. In particular, the directional and counterphase flickering stimuli were created by shifting the phase of the sine-wave grating composing the Gabor patch. For directional stimuli, the phase was shifted by ±90° every 40 ms. The counterphase flickering stimuli were created by shifting the phase 180° every 80 ms (Kanai & Verstraten, 2005; Pavan et al., 2009). This manipulation led to directionally ambiguous dynamic patterns (i.e., counterphase flickering) with the same temporal frequency of directional stimuli. On each trial, the starting phase of both adapting and test stimuli was randomized. The parameters of Gabor patches were selected according to the previous dMAE studies (e.g., Campana et al., 2011; Campana et al., 2013; Kanai & Verstraten, 2005; Pavan et al., 2009).

Our approach was based on collecting behavioral performance and EEG (electroencephalogram) activity simultaneously. We used a similar procedure to that employed by previous behavioral studies (Kanai & Verstraten, 2005; Oluk et al., 2016; Pavan et al., 2009). Each trial consisted of an adapting stimulus and a counterphase flickering test pattern (Fig. 1). As already mentioned above, the counterphase flickering patterns were directionally ambiguous with no net motion. The adapting stimulus was presented first and could be either drifting in one direction (directional adapter) or counterphase flickering (counterphase adapter). The counterphase adapter condition was used as a baseline (control) condition. The duration of the adapting stimulus was fixed in each experimental block and pseudo-randomly selected from two values: 640 ms (short adaptation) and 6.4 s (long adaptation). After an adapting-test blank interval of 80 ms (i.e., inter-stimulus interval; ISI), the counterphase flickering test Gabor was displayed for 320 ms. The short adaption duration, ISI and test duration values were selected based on previous research to achieve a robust rapid MAE (Kanai & Verstraten, 2005; Pavan et al., 2009). At the end of each trial, observers were requested to indicate, by a key press, whether the test pattern moved in the same or opposite direction to that of the adapting stimulus. They were also instructed to maintain fixation during each trial. After the keyboard press and a variable inter-trial interval (1-2 sec), during which only the fixation point was present, the next trial started.

Each experimental block consisted of 50 counterphase flickering and 50 directional (25 trials for each motion direction) adaptation trials. Each participant completed one experimental block for each adaptation duration and the order of these blocks was randomized across participants. Prior to these main EEG blocks, each participant was shown examples of visual stimuli followed by a practice (i.e., training) block for each adaptation duration. In these practice blocks, we used the same procedure but only collected behavioral data. Participants who reported the test pattern moving in the opposite direction of the adapter in the majority of directional trials were included in the following EEG experiment. This approach allowed us to include participants who performed the task according to our instructions and also experienced the motion adaptation illusion reliably for both duration conditions. During the main EEG sessions, participants performed the perceptual task for all the conditions, and upon debriefing, none of the participants reported any difficulty in performing the task.

2.4. EEG recording and preprocessing

EEG recording and preprocessing steps were similar to those described previously (Kaya & Kafaligonul, 2019; Kaya, Yildirim, & Kafaligonul, 2017). In brief, high-density EEG activity was recorded with a 64 channel MR-compatible system (Brain Products GmbH, Gilching, Germany). The placement of the cap electrodes was in accordance with a standard 10/20 system. Before the start of each experimental session, the EEG cap was carefully placed on each participant's head. A syringe with a blunt tip and q-tips was used to apply conductive paste (ABRALYT 2000 FMS, Herrsching–Breitbrunn, Germany) and to reduce impedances in each EEG channel. During each experimental session, the electrode impedance values were kept below 10 kΩ to reduce noise to a minimum. The AFz and FCz electrodes were used as ground and reference, respectively. EEG signals were sampled at 5 kHz and band-pass filtered between 0.016 and 250 Hz. EEG data, stimulus markers, and participant responses were stored on a secure hard disk via Vision Recorder Software (Brain Products, GmbH, Gilching, Germany) for further analyses.

Preprocessing of EEG data was carried out offline with BrainVision Analyzer 2.0 (BrainProducts, GmbH, Gilching, Germany). First, EEG signals were down-sampled to 500 Hz and filtered through Butterworth high-pass filter (0.5 Hz cut-off, 24 dB/octave), a 50 Hz notch

filter (50 Hz +/-2.5 Hz, 16th order) and a band-pass filter (1-50 Hz, 12 dB/octave). The data were also re-referenced to a common average and the cardioballistic artifacts were removed using the signal from the ECG channel (Allen, Polizzi, Krakow, Fish, & Lemieux, 1998). Afterwards, the data were segmented into epochs from 200 ms before the onset of the adapter to 1 sec after the offset of the test pattern. To remove common EEG artifacts (e.g., eye blinks, muscle artifacts, any residual heartbeat components), the data was further submitted to independent component analysis (ICA) using the Infomax algorithm. Last, artifact-contaminated trials (i.e., epochs) and bad channels were identified and removed through a combination of automated screening and manually by eye. In the automatic screening, any trial with oscillations over 50 μV/ms, a voltage change more than 200 μV or a change less than 0.5 μV in 100 ms was rejected. Bad channels were reconstructed using spherical spline interpolation (Perrin, Pernier, Bertrand, & Echallier, 1989). At the end of these standard preprocessing steps, on average 95% of trials were retained per condition.

2.5. ERP analyses

We averaged "cleaned" EEG signals across trials to compute event-related potentials (ERPs) time-locked to the onset of the test pattern. The ERPs were baseline corrected using the 200 ms pre-stimulus period before the onset of each adapter. It is possible that adapting stimuli can lead to changes in the evoked activity which are not specific to motion direction adaptation. These changes can also be dependent on the duration of adapters. To circumvent these potential confounds and to determine direction specific aftereffects on the evoked activity to the test pattern, we first subtracted the averaged ERPs of the counterphase trials from those of directional trials for each adaptation duration. We used these difference ERPs (directional – counterphase) for further statistical analyses. In fact, since counterphase flickering (i.e., directionally ambiguous) stimulation was used as a baseline (control) condition rather than a static visual flicker, the contribution of any confounding factor even after the test onset is expected to be limited. For instance, it is possible that the physical offset of the adapter may lead to evoked activity after the test onset due to the short ISI used between the adapter and test patterns. However, such offset response is expected to be highly similar in both directional and counterphase adapters. Accordingly, both directional and counterphase adapters should lead to

similar motion-offset evoked activities (Clarke, 1973; Kreegipuu & Allik, 2007) and the subtraction of ERPs for each adaptation duration is expected to eliminate this confound.

The spatiotemporal clusters associated with the changes in the difference ERPs were identified via a cluster-based permutation test integrated into Fieldtrip toolbox (Maris & Oostenveld, 2007; Oostenveld, Fries, Maris, & Schoffelen, 2011). This statistical test is a data-driven non-parametric framework to solve the problem of multiple comparisons (Type I error) and to cluster selected samples (electrode locations and time points) objectively. The difference ERPs of short and long adaptation conditions were compared by paired-sample t-tests at each time point and electrode location. All significant ($p < 0.05$) samples were clustered together based on temporal and spatial contiguity. Then, the cluster-level statistics were calculated by summing t-values within a cluster. A null-distribution of cluster-level statistics was created by randomly permuting the original data (i.e., assigning the original data to one of the two conditions) 10,000 times. The Monte Carlo method was used for these random-permutations. Finally, the observed cluster-level statistics were compared against the generated null-distribution. When the statistics of a spatiotemporal cluster in the real data fell in the highest or the lowest 2.5^{th} percentile of the null-distribution, the effect of adaptation duration ($long_{difference}$ vs. $short_{difference}$) was considered to be significant. Previous research using a warning stimulus and an imperative (i.e., test) stimulus revealed a component called contingent negative variation (CNV) over fronto-central scalp sites associated with expectancy (Walter, Cooper, Aldridge, McCallum, & Winter, 1964). Moreover, the amplitude of CNV component starting around 400 ms after the onset of the test stimulus has been found to be correlated with perceptual timing (Kononowicz & Penney, 2016; Li, Chen, Xiao, Liu, & Huang, 2017). Therefore, to overcome any unforeseen confounding factor and contamination due to the adapter, we performed the cluster-based permutation test within the first 400 ms after the onset of the test pattern. Following the cluster-based statistical analyses, we identified time windows and cluster of electrodes (i.e., exemplar sites) over which significant spatiotemporal clusters were mainly located. Using the identified exemplar sites, we displayed evoked activities of all conditions for illustrative purposes. Moreover, we averaged ERP amplitudes within the identified time windows over these locations and performed post-hoc paired and one-sample t-tests on these averaged amplitudes.

2.6. Source localization analyses

To locate the neural generators of the observed effects at the scalp level, we used the Standardized Low-Resolution Brain Electromagnetic Tomography (sLORETA) technique (Pascual-Marqui, 2002). sLORETA provides a three-dimensional discrete linear solution that has been shown to estimate the underlying cortical sources of scalp topographies with high and reliable localization accuracy (Hoffmann, Labrenz, Themann, Wascher, & Beste, 2014; Sekihara, Sahani, & Nagarajan, 2005). In its current version, the intra-cerebral volume is partitioned into 6239 voxels with 5 mm spatial resolution. The standardized current density of each voxel is calculated in a realistic head model using the MNI152 (Montreal Neurological Institute) template (Fuchs, Kastner, Wagner, Hawes, & Ebersole, 2002; Mazziotta et al., 2001). Here, we employed a similar approach to that used in previous research (e.g., Bluschke, Schuster, Roessner, & Beste, 2017). First, the source estimations for each participant and experimental condition were performed within the identified time window based on ERP analyses. Then, the differences between the voxel-wise normalized estimations of adapter types were computed (directional – counterphase) for each adaptation duration. These voxel-based sLORETA images were compared ($long_{difference}$ vs. $short_{difference}$) using the built-in voxel-wise randomization tests with 5000 permutations based on statistical non-parametric mapping (Nichols & Holmes, 2002).

3. Results

3.1. Behavioral results

The behavioral data are shown in Fig. 2. As in previous dMAE studies, the percentage of trials in which the test pattern was perceived to drift in the same direction to that of the adapting pattern is reported for all the adaptation conditions (Kanai & Verstraten, 2005; Pavan et al., 2009; Pavan et al., 2010). A percentage value above or below the chance level (50%) corresponds to either motion priming or aftereffect, respectively. The counterphase flickering adapters led to performance values around the chance level for both adaptation durations. On the other hand, the performance values for directional adapters were much lower than the chance level indicating robust motion aftereffects. A two-way repeated measures ANOVA with the adapter type (directional vs. counterphase) and duration (long vs. short) as factors, reported a significant effect of adapter type ($F_{1,18} = 76.298$, $p < 0.001$, $\eta_p^2 = 0.809$). The main effect of adaptation duration

was not significant ($F_{1,18}$ = 0.506, p = 0.486, η_p^2= 0.027), but the interaction between the adapter type and duration was significant ($F_{1,18}$ = 5.732, p = 0.028, η_p^2= 0.242).

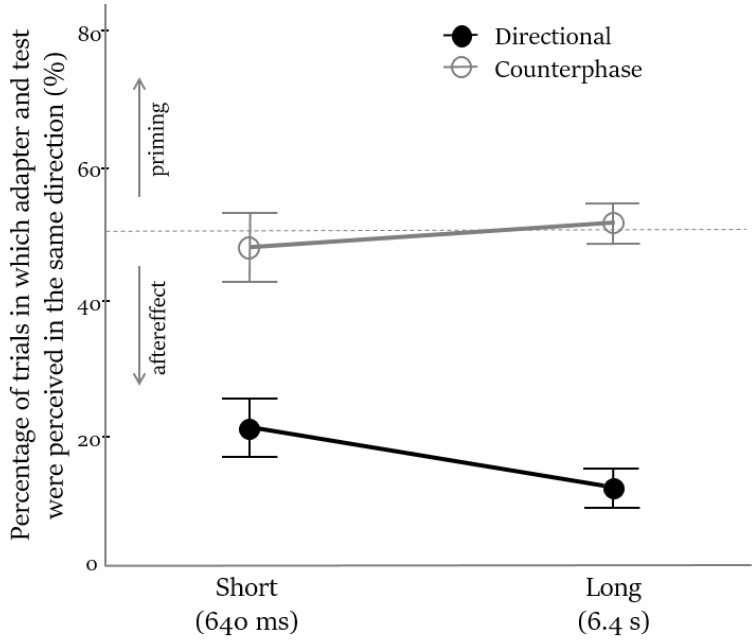

Fig. 2. Behavioral results (n=19). The percentage of trials, in which the adapter and test were perceived to move in the same direction, is displayed as a function of adapter duration. The open and filled circles correspond to the counterphase flickering and directional adapters, respectively. Error bars ± SEM.

Post-hoc pairwise comparisons revealed that the percentage value of directional adapter was significantly different than that of counterphase flickering at each duration level (short: t_{18} = -5.564, p < 0.001, Cohen's d = 1.306; long: t_{18} = -8.924, p < 0.001, Cohen's d = 3.065). In terms of percentage values, a significant difference between the short and long conditions of directional adaptation was also found to be significant (t_{18} = -2.709, p = 0.014, Cohen's d = 0.569). On the other hand, there was no difference between the counterphase flickering conditions (t_{18} = 0.629, p = 0.537, Cohen's d = 0.196). Overall, this suggests that both adaptation durations led to significant motion aftereffects (i.e., directional – counterphase difference) but the aftereffect induced by the longer duration was significantly stronger.

3.2. Motion aftereffects on the evoked activity

In line with behavioral results, we found robust changes in the evoked activity to the test pattern. A cluster-based permutation test on the difference (directional – counterphase) ERPs revealed a significant effect of duration ($long_{difference}$ vs. $short_{difference}$). The significant spatiotemporal cluster (cluster-level t_{sum} = 2558.5, p = 0.003) associated with this effect was within 64-112 ms time

range and mainly located over occipital and parieto-occipital scalp sites (Fig. 3). The cluster also included some of the parietal and centro-parietal electrodes. At these significant scalp sites, the averaged difference (directional – counterphase) potentials of long adaptation were higher than those of short adaptation duration. In agreement with behavioral results, this indicates a significant interaction between adapter type and duration over these regions. The cluster-based permutation test also pointed out an earlier (6-32 ms time range) and a later (212-230 ms time range) cluster. However, these spatiotemporal clusters did not lead to a significant effect (early: cluster-level t_{sum} = 730.87, p = 0.113; late: cluster-level t_{sum} = 146.57, p = 0.503).

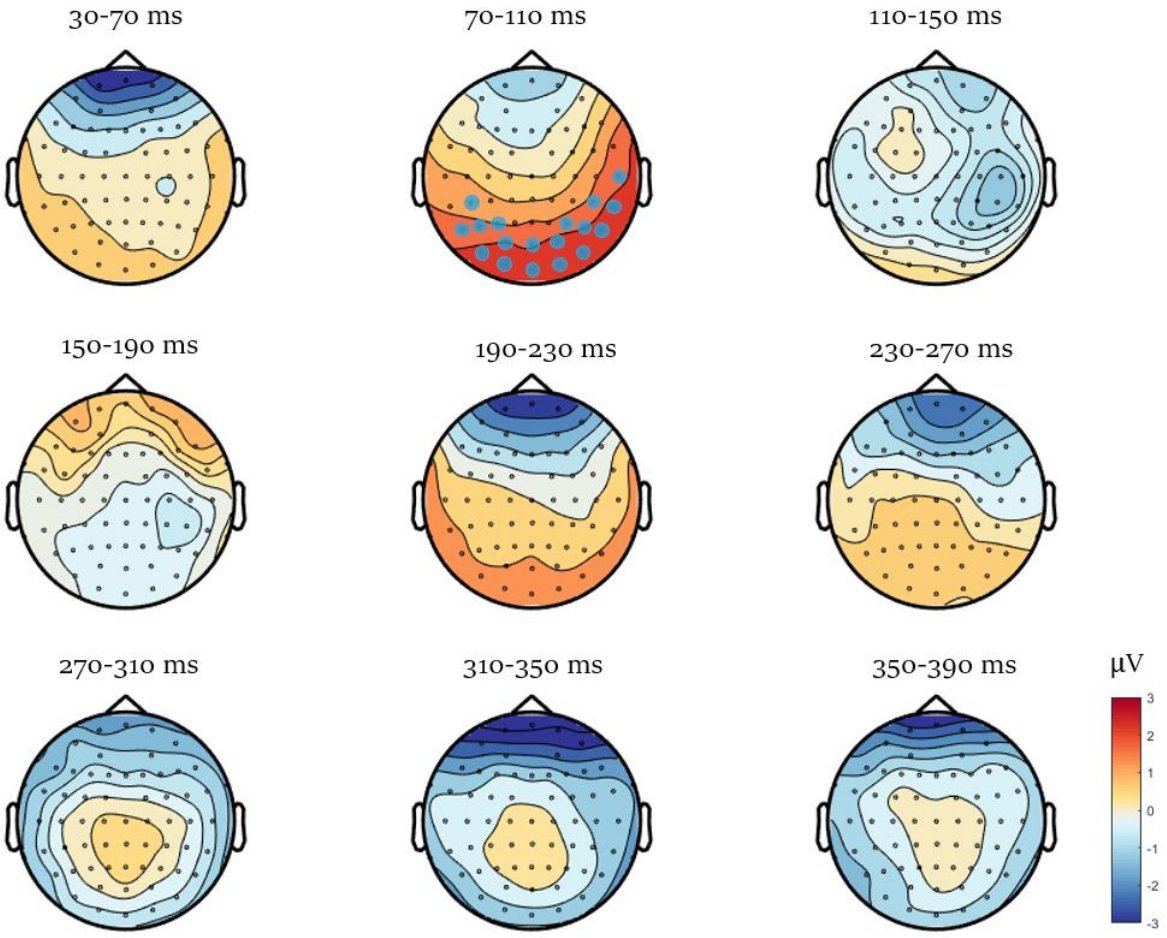

Fig. 3. Results of the cluster-based permutation test comparing the difference (directional – counterphase) ERPs of the long adaptation duration to those of short condition ($long_{difference}$ vs. $short_{difference}$). Voltage topographical maps of the grand averaged waveforms ($long_{difference}$ – $short_{difference}$) are shown within 40 ms time windows. The electrodes, which were part of the significant spatiotemporal cluster throughout each 40 ms time window, are marked by blue filled circles on the topographical maps. These marked electrodes are *O1, Oz, O2, PO7, PO3, POz, PO4, PO8, P7, P5, P3, P4, P6, P8, CP5, CP6, TP8, T8.*

To understand the functional and neuroanatomical sources underlying this significant effect, we performed source estimations within the 64-112 ms time window (Fig. 4). The sLORETA analyses comparing the differences across adaptation durations suggested that this effect was dominant in the left hemisphere and was associated with the activation changes in the cuneus and middle occipital gyrus (Brodmann areas 17, 18 and 19). We also found a relatively small cluster of sources located in the precuneus and superior occipital gyrus.

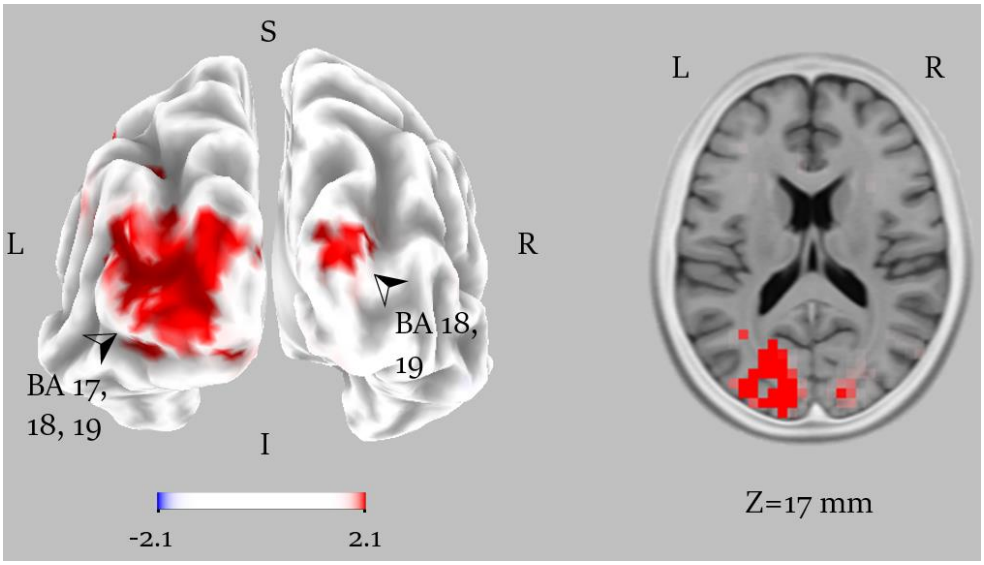

Fig. 4. Whole-brain t-value maps from sLORETA source estimations within the 64-112 ms time range. Viewing angle of the 3D inflated brain template on the left was arranged according to the significant scalp sites. To better observe the cortical depth, a horizontal slice (T2 MNI-template ‘‘Colin 27’’ of sLORETA) positioned at a coordinate of Z= 17 mm is also displayed on the right side. The color bar below represents voxel t-values. The sign of the difference between derived waveforms is represented by negative (blue) and positive (red) t-values. Scaling was arranged so that shaded colors indicate (extreme) t-values above 2.1 or below -2.1.

To display evoked activities to the test pattern and the aftereffects on these activities for illustrative purposes, we computed averaged potentials for the electrodes (i.e., exemplar sites) marked in Fig. 3. As shown by the averaged potentials of these electrodes in Fig. 5A, the test pattern elicited robust components peaking around 50 ms (C1), 120 ms (P1) and 220 ms (N1). Both C1 and P1 components were mainly evident over occipital and parieto-occipital electrodes (Supplementary Fig. S1). Although the P1 component was present in all the conditions, the C1 component was present and quite robust only in the long adaptation conditions. In terms of difference ERPs, the averaged activities of the long condition were higher within each of these

component ranges (Fig. 5B). However, as mentioned above, the differential effects of the adapter type (directional – counterphase) for each adaptation duration only led to a significant spatiotemporal cluster within late C1 and early P1 component range (64-112 ms time range). While the difference ERP of the long condition was located over lateral parieto-occipital and parietal electrodes in this time range, the difference ERP of the short condition was mainly located over the occipital electrodes (Fig. 5C).

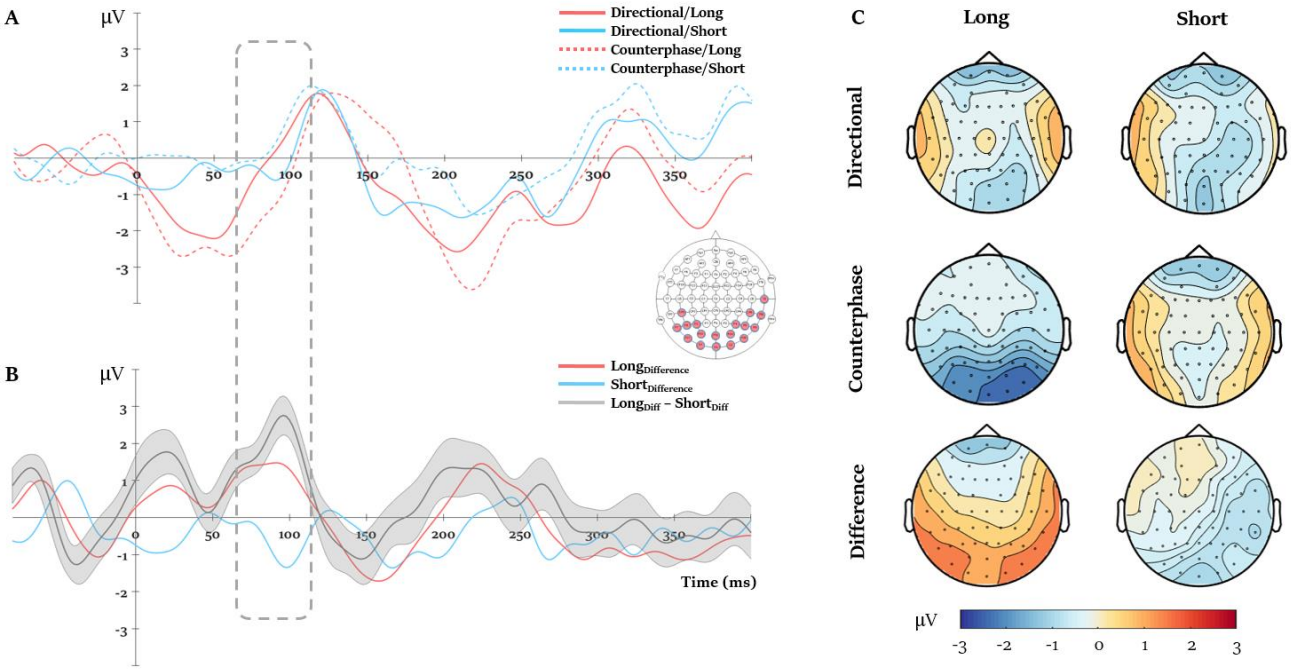

Fig. 5. (A) Averaged activities and derived waveforms from the exemplar scalp site. The exemplar site included all the marked electrodes on a head model (*O1, Oz, O2, PO7, PO3, POz, PO4, PO8, P7, P5, P3, P4, P6, P8, CP5, CP6, TP8, T8*). The averaged ERPs for different adaptation conditions. The ERPs were time-locked to the onset of the test pattern and displayed in the range from -80 ms (i.e., the onset of the blank interval between adapter and test) to 400 ms. The identified time window based on the cluster-based permutation test is highlighted by a dashed rectangle. (B) The difference waveforms between conditions. The gray shaded area in the final derived waveform ($long_{difference}$ – $short_{difference}$) represents the standard error (±SEM) across participants. Other conventions are the same as those in the panel above. (C) Voltage topographical maps of the grand averaged waveforms within the identified time window (64-112 ms). The voltage topographical map of each adapter type and duration condition is shown in separate rows and columns. The difference topographical maps (directional-counterphase) are shown at the bottom row.

Post-hoc pairwise comparisons on the averaged difference potentials within this range confirmed the significant difference between the two adaptation durations ($long_{difference}$ vs. $short_{difference}$; t_{18} = 4.78, $p < 0.001$, Cohen's d = 1.37). Hence, this also indicated a significant interaction between the adapter type and duration. To understand the nature of this interaction, we further compared the average potentials of the directional condition with that of the counterphase at each duration (i.e., directional vs. counterphase). Compared to the counterphase, the average potential of the directional condition was significantly higher for the long condition (t_{18} = 4.02, p = 0.002, Cohen's d = 0.92). On the other hand, the changes in the average potentials were in the opposite direction for the short condition and they were not significant (t_{18} = -2.03, p = 0.058, Cohen's d = 0.47).

Using the coordinates by previous research (Beckers & Zeki, 1995; Campana et al., 2011; Watson et al., 1993) and the electrodes in Fig. 5, we identified two sub-clusters (ROIs) mainly located over occipital and parietal electrodes. These occipital and parietal ROIs corresponded to early visual areas (primary visual cortex and neighboring areas) and V5/MT (and also neighboring parietal regions), respectively (Supplementary Table S1). It should also be noted that the occipital ROI included electrodes at the center of the significant spatiotemporal cluster. The averaged activities over these ROIs were highly similar (Fig. 6). For both ROIs, there was a significant difference between adaptation durations ($long_{difference}$ vs. $short_{difference}$, Table 1) and the average potential of directional condition was significantly higher than that of counterphase (i.e., directional vs. counterphase) for the long adaptation duration. However, the average potentials of short duration were significantly different only for the occipital ROI (t_{18} = -2.27, p = 0.036, Cohen's d = 0.52). There was no such difference for the other parietal ROI (t_{18} = -1.63, p = 0.120, Cohen's d = 0.37). Overall, these additional analyses suggest that the short-term motion aftereffects were dominant over occipital scalp sites corresponding to low-level visual areas.

It is interesting to observe that the waveforms in Fig. 5A also indicate a duration aftereffect not specific to motion adaptation (i.e., adapter type). We additionally performed a cluster-based permutation test to explore the main effect of adaptation duration. We combined (i.e., averaged)

the ERPs of two adapter types and then, compared these two combined waveforms across adaptation durations using a cluster-based permutation test ($long_{combined}$ vs. $short_{combined}$). This test revealed a significant effect of duration (cluster-level t_{sum} = -3730.3, p = 0.003) only within the C1 component range (10-75 ms). The C1 amplitudes of short adaptation durations were greater than those of long conditions. The significant spatiotemporal cluster was mainly clustered over occipital and parieto-occipital sites (Supplementary Fig. S2 and S3) and included most of the exemplar electrodes shown in Fig. 5.

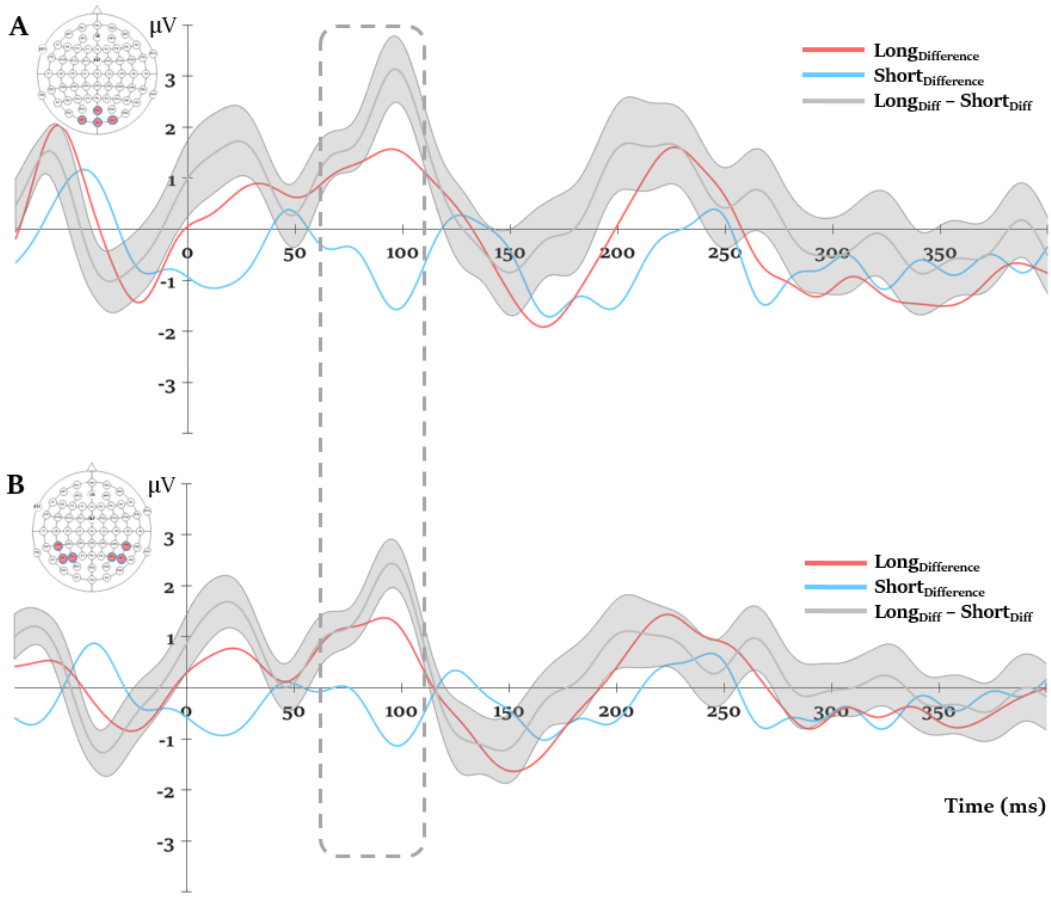

Fig. 6. Averaged difference potentials across the occipital (A) and parietal (B) ROIs. The electrode locations are shown on the left insets. The activities were time-locked to the onset of the test pattern and displayed in the range from -80 ms (i.e., the onset of the blank interval between adapter and test) to 400 ms. The identified time window based on the cluster-based permutation test is highlighted by a dashed rectangle. The gray shaded area in the final derived waveform ($long_{difference}$ − $short_{difference}$) represents the standard error (±SEM) across participants. Other conventions are the same as those in Fig. 5B.

Table 1. The results of the post-hoc t-tests and descriptive statistics for the occipital and parietal ROIs. The values of each ROI are grouped in separate rows. For each ROI, the comparison of difference potentials across adaptation durations ($long_{difference}$ vs. $short_{difference}$) is shown first. Then, the statistical results comparing directional and counterphase conditions (i.e., directional vs. counterphase) condition at each adaptation duration are shown in the following rows. Significant *p* values ($p < 0.05$) are highlighted in bold.

	t_{18}	*p*	Cohen's d	Mean (μV)	SEM (μV)
Occipital ROI					
$Long_{diff}$ vs. $Short_{diff}$	4.357	**<0.001**	1.316	2.201	0.505
$Long_{diff}$	3.481	**0.003**	0.798	1.324	0.380
$Short_{diff}$	-2.268	**0.036**	0.520	-0.877	0.387
Parietal ROI					
$Long_{diff}$ vs. $Short_{diff}$	4.463	**<0.001**	1.260	1.635	0.366
$Long_{diff}$	4.102	**0.001**	0.941	1.106	0.270
$Short_{diff}$	-1.634	0.120	0.375	-0.528	0.323

4. Discussion

In the present study, we investigated short- and long-term forms of dynamic motion aftereffect (dMAE) using both psychophysical and EEG techniques. Behavioral results indicated that both adaptation durations led to aftereffects, but the aftereffects by the long-term were significantly stronger. Accordingly, having the adaptation duration (i.e., long vs. short) as a critical experimental factor, we identified scalp sites and ERP components. The adaptation duration significantly influenced aftereffects on the evoked activity within the 64-112 ms time range (between the late C1 and early P1) and mainly over occipital and parieto-occipital electrodes. These findings suggest that dMAE takes place over visual areas that play a significant role in low- and mid-level of motion processing. Thus, they provide important electrophysiological evidence for previous behavioral and brain stimulation (TMS) results (Campana et al., 2011; Campana et al., 2013; Pavan et al., 2009).

Our study is the first systematic EEG investigation on the rapid form of (dynamic) MAE and also provides novel insights into the nature of this adaptation. In particular, specific comparisons between short and long adaptation durations revealed important information about this type of

motion adaptation. The additional ERP analyses indicated that short adaptation gives rise to significant aftereffects mainly over occipital scalp sites. On the other hand, the significant aftereffects of the long adaptation duration were present over both occipital and parietal electrodes. This suggests that the recruitment of early visual areas for the dMAE also depends upon the timescale used. Previously, Campana et al. (2011) found that rapid MAE is strongly reduced when either areas V2/V3 or V5/MT are disrupted with repetitive TMS. However, the stimulation targeted to V2/V3 weakened rapid motion aftereffect much more than V5/MT stimulation did. Our results are in agreement with these findings by pointing out the important and causal involvement of low-level visual areas in rapid MAE. Moreover, our results highlight the distinct nature of aftereffects induced by each adaptation duration. Compared to the baseline condition (i.e., counterphase flickering), the directional adapters led to aftereffects on the evoked activity in the opposite direction for each duration. In other words, the rapid MAE on the evoked activity were in the opposite direction, emphasizing the distinct characteristics and nature of rapid MAE. Building from these findings, one can hypothesize that rapid MAE may lead to distinct sensory plasticity and engage different neural mechanisms even in the same cortical area. This hypothesis is also supported by previous models of rapid and long MAEs. Using a modified and extended version of Adelson-Bergen motion energy sensors, Pavan, Contillo and Mather (2013, 2014) systematically investigated the effect of adaptation duration on MAEs. To account for adaptation effects over different timescales, these sensors included multi-stage leaky integrators. Their simulation results revealed that the amount of time needed by the motion sensor to lose most of its gain and approach the asymptotic baseline activation is a key factor to identify distinct characteristics of rapid and long MAEs. They further reported that the first-order leaky integrator was sufficient to implement adaptation effects of long durations which can span many seconds. However, a second-order leaky integrator, which causes the sensor to require a finite amount of time to react to a sudden change in stimulation, was critical for the rapid form of MAE (Pavan et al., 2014). These findings clearly demonstrate that the neural mechanisms operating over different timescales can be supported and recruited in the same neural substrate. According to Pavan et al. (2014) and previous research (e.g., Wark, Fairhall, & Rieke, 2009), the temporal dynamics of adaptation may reflect a balance between adapting rapidly to avoid short-term saturation and adapting slowly (over longer timescales) to avoid instability in the absence of changes in image statistics. This is because changes in natural scenes occur over multiple

timescales, therefore short- and long-term adaptations in the visual system might be expected to occur over a correspondingly diverse range of timescales.

Previous EEG recordings on motion adaptation were mainly based on monitoring changes in motion-onset visual evoked potentials (i.e., motion-onset VEPs). In motion-onset VEP paradigms, the motion specific potentials are identified by comparing the cortical activities to a motion display with those to the preceding stationary period of the same stimulus (see Kuba, Kubová, Kremláček, & Langrová, 2007 for a review). In the adaptation experiments of motion-onset VEP paradigm, an adapter moving in a specific direction was typically displayed for a few seconds and then the test stimulus was shown. However, to identify aftereffects on the motion-onset VEPs, the test stimulus included both a stationary and a coherently moving period. These studies consistently reported aftereffects on a negative component peaking around 150-200 ms time range (e.g., Bach & Ullrich, 1993; Hoffmann, Dorn, & Bach, 1999). This motion specific component, which is also known as N2 component, has been associated with the activity of human area V5/MT+ (Heinrich, 2007; Nakamura & Ohtsuka, 1999). To some extent, the aftereffects on this component were also found to be direction specific (Heinrich, Renkl, & Bach, 2005; Hoffmann, Unsöld, & Bach, 2001). Relatively more comparable experimental designs to the present EEG study have been used in recent neurophysiological recordings in area MT (Kar, Duijnhouwer, & Krekelberg, 2017; Kar & Krekelberg, 2016). During each trial of these recordings, a 3 sec adaptation period was used and after a blank interval (300 ms) a test pattern was displayed for 300 ms. Similar to our experiment, directional or dynamic adapters with no net directional motion (i.e., random-dot kinematograms with either 100% or 0% coherence level) were used. However, the test pattern was always directional. The long conditions of the current study are comparable in terms of adaptation duration and types. They reported adaptation induced modulations over the evoked local field potentials (LFPs) in 50-70 ms and 90-110 ms time ranges. Furthermore, these modulations were specific to motion direction and the later modulations were stronger. Compared to the previous motion-onset VEP experiments, these findings point to earlier aftereffects on the evoked activity and they are highly similar to the time range observed here. To some extent, our EEG recordings for the long adaptation durations confirm these modulations in the LFP activities. It is important to note that rapid MAE can only be generated with dynamic ambiguous test patterns (e.g., counterphase flickering) but not with

stationary test patterns (Pavan & Skujevskis, 2013). Therefore, future neurophysiological recordings systematically investigating the effect of different test patterns (static, dynamic/directionally ambiguous and directional) on these early modulations will be informative to further extend our understanding of the mechanisms and principles underlying rapid MAE.

Interestingly, our results also indicated duration aftereffects (not specific to the adapter type) on the C1 component. In both directional and counterphase adapters of the long condition, the average potentials were lower within the C1 range. On the other hand, the C1 component was almost absent for the short adaptation conditions and the average potentials were close to the baseline level. In a recent study, Kaya et al. (2017) systematically examined the evoked activity to a visual apparent motion under different time interval adaptation conditions. Their design included both auditory and visual sub-second time interval conditions. Moreover, they defined two main adaptation conditions (short vs. long) which were shorter and longer than the time interval demarcated by the apparent motion frames. Similar to our findings here, they found significant aftereffects on the C1 component within 50-80 ms time range. For visual time interval adaptations, the average potential of long condition was lower than that of the short. On the other hand, the aftereffects by auditory time intervals were in the opposite direction such that the short adaptations resulted in lower average potentials. In addition to time interval aftereffects within the C1 component range, these findings further indicated that these aftereffects were distinct for each modality. It is well established that C1 component receives major contributions from the earliest retinotopic regions of the visual processing and this component is associated with the early processing over primary visual cortex (V1) of Brodmann area 17 (Clark, Fan, & Hillyard, 1995; Di Russo, Martinez, & Hillyard, 2003). In line with these basic features, the C1 component has been found to be sensitive to low-level visual manipulations (Baseler & Sutter, 1997; Foxe et al., 2008). By showing duration and time interval aftereffects on this component, the current and previous EEG findings within the context of visual motion suggest that C1 component may be also linked to timing and temporal processing. Indeed, this fits well with previous behavioral results showing that duration aftereffects on perceived timing are narrowly tuned to the location of the visual adapters and hence spatially specific (Ayhan, Bruno, Nishida, & Johnston, 2009; Bruno, Ayhan, & Johston, 2010; Johnston, Arnold, & Nishida, 2006). Using a series of additional manipulations in the visual domain, it was also demonstrated that low-level mechanisms play an

important role in encoding the duration of visual events in a retinotopic frame of reference (see Bruno & Cicchini, 2016 for a review). Moreover, there is recent TMS evidence suggesting that temporal information at V1 and V5/MT is encoded in retinotopic spatial frames (Fortunato, Kénel-Pierre, Murray, & Bueti, 2018). On the other hand, it is still possible that other factors may have contaminated the main effect of duration adaptation on the C1 component. For instance, previous research also pointed out that the C1 component may be modulated by attention under some circumstances (Baumgartner, Graulty, Hillyard, & Pitts, 2018a; Baumgartner, Graulty, Hillyard, & Pitts, 2018b; Kelly, Gomez-Ramirez, & Foxe, 2008). Future experiments designed to control other factors (e.g., attention) and to specifically understand the role of C1 component modulations in visual timing and time perception will be informative.

5. Conclusions

To conclude, the current findings indicate that dynamic motion aftereffects take place over ERP components at occipital and parieto-occipital scalp sites. Thus, they provide electrophysiological evidence that dynamic motion aftereffects tap both low- and mid-level motion sensors. In terms of scalp sites and the direction of modulations, our data further showed some distinct characteristics of aftereffects by short- and long-term directional adapters. Accordingly, these findings, in conjunction with a variety of related converging evidence, support the general view that sensory plasticity is an active time-dependent process which involves different mechanisms.

Funding

This work was supported by the British Academy via Newton Mobility Grants (grant number 1072261).

Declaration of interest

The authors declare no conflict of interest.

Open Practices

The data, materials and code of the study have been made publicly available via the Open Science Framework and can be accessed at https://osf.io/4f2uw/

Acknowledgements

We would like to express our special thanks to Dr. Aaron Michael Clarke for suggestions on the ERP analyses. We are also grateful to Soheil Taraghinia and Mert Ozkan for technical assistance in data collection.

REFERENCES

Allen, P.J., Polizzi, G., Krakow, K., Fish, D.R. & Lemieux, L. (1998). Identification of EEG events in the MR scanner: The problem of pulse artifact and a method for its subtraction. NeuroImage, 8, 229–239.

Ayhan, I., Bruno, A., Nishida, S., & Johnston, A. (2009). The spatial tuning of adaptation-based time compression. Journal of Vision, 9(11):2, 1–12.

Bach, M., & Ullrich, D. (1994). Motion adaptation governs the shape of motion-evoked cortical potentials. Vision Research, 34(12), 1541-1547.

Baseler, H.A., & Sutter, E.E. (1997). M and P components of the VEP and their visual field distribution. Vision Research, 37, 675– 690.

Baumgartner, H.M., Graulty, C.J., Hillyard, S.A., & Pitts, M.A. (2018), Does spatial attention modulate the C1 component? Cognitive Neuroscience, 9 (1-2), 4-19.

Baumgartner, H.M., Graulty, C.J., Hillyard, S.A., & Pitts, M.A. (2018), Does spatial attention modulate the C1 component? The jury continues to deliberate. Cognitive Neuroscience, 9 (1-2), 34-37.

Beckers, G., & Zeki, S. (1995). The consequences of inactivating areas V1 and V5 on visual motion perception. Brain, 118(1), 49-60.

Bluschke, A., Schuster, J., Roessner, V., & Beste, C. (2017). Neurophysiological mechanisms of interval timing dissociate inattentive and combined ADHD subtypes. Scientific Reports, 8:2033.

Brainard, D. (1997). The psychophysics toolbox. Spatial Vision, 10, 433–436.

Bruno, A., Ayhan, I., & Johnston, A. (2010). Retinotopic adaptation-based visual duration compression. Journal of Vision, 10 (10): 30, 1-18.

Bruno, A., & Cicchini, G.M. (2016). Multiple channels of visual time perception. Current Opinion in Behavioral Sciences, 8, 131–139.

Campana, G., Maniglia, M., & Pavan, A. (2013). Common (and multiple) neural substrates for static and dynamic motion after-effects: A rTMS investigation. Cortex, 49(9), 2590–2594.

Campana, G., Pavan, A., Maniglia, M., & Casco, C. (2011). The fastest (and simplest), the earliest: The locus of processing of rapid forms of motion aftereffect. Neuropsychologia, 10, 2929–2934.

Clark, V.P., Fan, S., & Hillyard, S.A. (1995). Identification of early visual evoked potential generators by retinotopic and topographic analyses. Human Brain Mapping, 2, 170–187.

Clarke, P.G.H. (1973). Visual evoked potentials to changes in themotion of a patterned field. Experimental Brain Research, 18, 145-155.

Clifford, C.W.G. (2002). Perceptual adaptation: motion parallels orientation. Trends in Cognitive Science, 6, 136–143.

Culham, J.C., Verstraten, F.A., Ashida, H., & Cavanagh, P. (2000). Independent aftereffects of attention and motion. Neuron, 28, 607-615.

Di Russo, F., Martinez, A., & Hillyard, S.A. (2003). Source analysis of event-related cortical activity during visuo-spatial attention. Cerebral Cortex, 13(5), 486–499.

Faul, F., Erdfelder, E., Buchner, A., & Lang, A.-G. (2009). Statistical power analyses using G*Power 3.1: tests for correlation and regression analyses. Behavioural Research Methods, 41, 1149-1160.

Fortunato, G., Kénel-Pierre, T., Murray, M., & Bueti, D. (2018). The spatial representation of time in visual cortex. Journal of Vision, 18(10), 961-961.

Foxe, J.J., Strugstad, E.C., Sehatpour, P., Molholm, S., Pasieka, W., Schroeder, C. E., et al. (2008). Parvocellular and magnocellular contributions to the initial generators of the visual evoked potential: High- density electrical mapping of the “C1” component. Brain Topography, 21, 11– 21.

Fuchs, M., Kastner, J., Wagner, M., Hawes, S., & Ebersole, J.S. (2002). A standardized boundary element method volume conductor model. Clinical Neurophysiology, 113, 702–712.

Glasser, D.M., Tsui, J.M., Pack, C.C., & Tadin, D. (2011). Perceptual and neural consequences of rapid motion adaptation. Proceedings of the National Academy of Sciences USA, 108(45), E1080-E1088.

Heinrich, S.P. (2007). A primer on motion visual evoked potentials. Documenta Ophthalmologica, 114(2), 83–105.

Heinrich, S.P., Renkl, A.E.H., Bach, M. (2005). Pattern specificity of human visual motion processing, Vision Research, 45, 2137-2143.

Hoffmann, M., Dorn, T. J., & Bach, M. (1999). Time course of motion adaptation: motion-onset visual evoked potentials and subjective estimates. Vision Research, 39(3), 437-444.

Hoffmann, S., Labrenz, F., Themann, M., Wascher, E., & Beste, C. (2014). Cross linking EEG time-frequency decomposition and fMRI in error monitoring. Brain Structure and Function, 219, 595–605.

Hoffmann, M.B., Unsöld, A.S., & Bach, M. (2001). Directional tuning of human motion adaptation as reflected by the motion VEP. Vision Research, 41, 2187–2194.

Johnston, A., Arnold, D.H., & Nishida, S. (2006). Spatially localized distortions of event time. Current Biology, 16(5), 472–479.

Kanai, R., & Verstraten, F.A. (2005). Perceptual manifestations of fast neural plasticity: Motion priming, rapid motion aftereffect and perceptual sensitization. Vision Research, 45: 3109-3116.

Kar, K., Duijnhouwer, J., & Krekelberg, B. (2017). Transcranial alternating current stimulation attenuates neuronal adaptation. Journal of Neuroscience, 37, 2325–2335.

Kar, K., & Krekelberg, B. (2016). Testing the assumptions underlying fMRI adaptation using intracortical recordings in area MT. Cortex, 80, 21–34.

Kaya, U., & Kafaligonul, H. (2019). Cortical processes underlying the effects of static sound timing on perceived visual speed. NeuroImage, 199, 194-205.

Kaya, U., Yildirim, F.Z., & Kafaligonul, H. (2017). The involvement of centralized and distributed processes in sub-second time interval adaptation: An ERP investigation of apparent motion. European Journal of Neuroscience, 46, 2325–2338.

Kelly, S.P., Gomez-Ramirez, M., & Foxe, J.J. (2008). Spatial attention modulates initial afferent activity in human primary visual cortex. Cerebral Cortex, 18, 2629–2636.

Kobayashi, Y., Yoshino, A., Ogasawara, T., & Nomura, S. (2002). Topography of evoked potentials associated with illusory motion perception as a motion aftereffect. Cognitive Brain Research, 13, 75-84.

Kononowicz, T.W., & Penney, T.B. (2016). The contingent negative variation (CNV): Timing isn't everything. Current Opinion in Behavioral Sciences, 8, 231–237.

Kohn, A. (2007). Visual adaptation: Physiology, mechanisms, and functional benefits. Journal of Neurophysiology, 97(5), 3155-3164.

Kohn, A., & Movshon, J.A. (2003). Neuronal adaptation to visual motion in area MT of the macaque. Neuron, 39(4), 681-691.

Kreegipuu, K., & Allik, J. (2007). Detection of motion onset and offset: Reaction timeand visual evoked potential analysis.Psychological Research,71, 703–708.

Krekelberg, B., Boynton, G., & Van Wezel, R. (2006). Adaptation: From single cells to BOLD signals. Trends in Neurosciences, 29(5), 250-256.

Kuba, M., Kubová, Z., Kremláček, J., & Langrová, J. (2007). Motion-onset VEPs: Characteristics, methods, and diagnostic use. Vision Research, 47(2), 189-202.

Li, B., Chen, Y., Xiao L., Liu, P. & Huang, X. (2017) Duration adaptation modulates EEG correlates of subsequent temporal encoding. NeuroImage, 147, 143–151.

Maris, E., & Oostenveld, R. (2007). Nonparametric statistical testing of EEG- and MEG-data. Journal of Neuroscience Methods, 164 (1), 177–190.

Mather, G., Pavan, A., Campana, G., & Casco, C. (2008). The motion aftereffect reloaded. Trends in Cognitive Science, 12, 481-487.

Mazziotta, J., Toga, A., Evans, A., Fox, P., Lancaster, J., Zilles, K., et al. (2001). A probabilistic atlas and reference system for the human brain: International consortium for brain mapping (ICBM). Philosophical Transactions of Royal Society B Biological Sciences, 356, 1293–1322.

Nakamura, Y., & Ohtsuka, K. (1999). Topographical analysis of motion-triggered visual-evoked potentials in man. Japanese Journal of Ophthalmology, 43(1), 36-43.

Nichols, T.E., & Holmes, A.P. (2002). Nonparametric permutation tests for functional neuroimaging: A primer with examples. Human Brain Mapping, 15, 1–25.

Nishida, S., & Sato, T. (1995). Motion aftereffect with flickering test patterns reveals higher stages of motion processing. Vision Research, 35, 477-490.

Oluk, C., Pavan, A., & Kafaligonul, H. (2016). Rapid motion adaptation reveals the temporal dynamics of spatiotemporal correlation between ON and OFF pathways. Scientific Reports, 6, 34073.

Oostenveld, R., Fries, P., Maris, E., & Schoffelen, J.M. (2011). FieldTrip: Open source software for advanced analysis of MEG, EEG, and invasive electrophysiological data. Computational Intelligence and Neuroscience, 2011, 156869.

Pascual-Marqui, R.D. (2002). Standardized low-resolution brain electromagnetic tomography (sLORETA): technical details. Methods and Findings in Experimental and Clinical Pharmacology, 24 (Suppl. D), 5–12.

Pavan, A., Campana, G., Guerreschi, M., Manassi, M., & Casco, C. (2009). Separate motion detecting mechanisms for first- and second-order patterns revealed by rapid forms of visual motion priming and motion aftereffect. Journal of Vision, 9(11):27, 1-16.

Pavan, A., Campana, G., Maniglia, M., & Casco, C. (2010). The role of high-level visual areas in short- and longer-lasting forms of neural plasticity. Neuropsychologia, 48, 3069-3079.

Pavan, A., Contillo, A., & Mather, G. (2013). Modelling adaptation to directional motion using the Adelson-Bergen energy sensor. PLoS ONE, 8(3), e59298.

Pavan, A., Contillo, A., & Mather, G. (2014). Modelling fast forms of visual neural plasticity using a modified second-order motion energy model. Journal of Computational Neuroscience, 37(3), 493-504.

Pavan, A., & Skujevskis, M. (2013). The role of stationary and dynamic test patterns in rapid forms of motion after-effect. Journal of Vision, 13(1):10, 1-17.

Perrin, F., Pernier, J., Bertrand, O., & Echallier, J.F. (1989). Spherical splines for scalp potential and current density mapping. Electroencephalography and Clinical Neurophysiology, 72, 184–187.

Pelli, D. (1997). The VideoToolbox software for visual psychophysics: Transforming numbers into movies. Spatial Vision, 10, 437–442.

Priebe, N.J., Churchland, M.M., & Lisberger, S.G. (2002). Constraints on the source of short-term motion adaptation in macaque area MT. I. The role of input and intrinsic mechanisms. Journal of Neurophysiology, 88(1), 354-369.

Priebe, N.J., & Lisberger, S.G. (2002). Constraints on the source of short-term motion adaptation in macaque area MT. II. Tuning of neural circuit mechanisms. Journal of Neurophysiology, 88(1), 370-382.

Sekihara, K., Sahani, M., & Nagarajan, S.S. (2005). Localization bias and spatial resolution of adaptive and non-adaptive spatial filters for MEG source reconstruction. NeuroImage, 25, 1056–1067.

Walter, W.G, Cooper, R., Aldridge, V.J., McCallum, W.C. & Winter, A.L. (1964) Contingent negative variation: An electric sign of sensorimotor association and expectancy in the human brain. Nature, 203 (4943), 380–384.

Wark, B., Fairhall, A., & Rieke, F. (2009). Timescales of inference in visual adaptation. Neuron, 61(5), 750–761.

Watson, J.D., Myers, R., Frackowiak, R.S., Hajnal, J.V., Woods, R.P., Mazziotta, J.C. et al. (1993). Area V5 of the human brain: Evidence from a combined study using positron emission tomography and magnetic resonance imaging. Cerebral Cortex, 3(2), 79-94.

World Medical Association (2013). Declaration of Helsinki: Ethical principles for medical research involving human subjects. Journal of the American Medical Association, 310 (20), 2191–2194.

CRediT authorship contribution statement

Sibel Akyuz: Conceptualization; Data curation; Formal analysis; Investigation; Methodology; Visualization; Writing - original draft. **Andrea Pavan:** Conceptualization; Methodology; Funding acquisition; Supervision; Writing - review & editing. **Utku Kaya:** Formal analysis; Visualization; Writing - review & editing. **Hulusi Kafaligonul:** Conceptualization; Formal analysis; Visualization; Funding acquisition; Supervision; Writing - review & editing.

SUPPLEMENTARY DATA

Supplementary Table S1. Electrodes designated for the region of interests (ROIs). In the first column, the marked electrodes in Fig. 3 are listed. The selected electrodes for the occipital and parietal ROIs are listed in the second and third columns, respectively.

	Significant Electrodes	Occipital ROI	Parietal ROI
Electrodes	O1, Oz, O2, PO7, PO3, POz, PO4, PO8, P7, P5, P3, P4, P6, P8, CP5, CP6, TP8, T8	POz, O1, Oz, O2	Cp5, Cp6, P5, P6, P3, P4

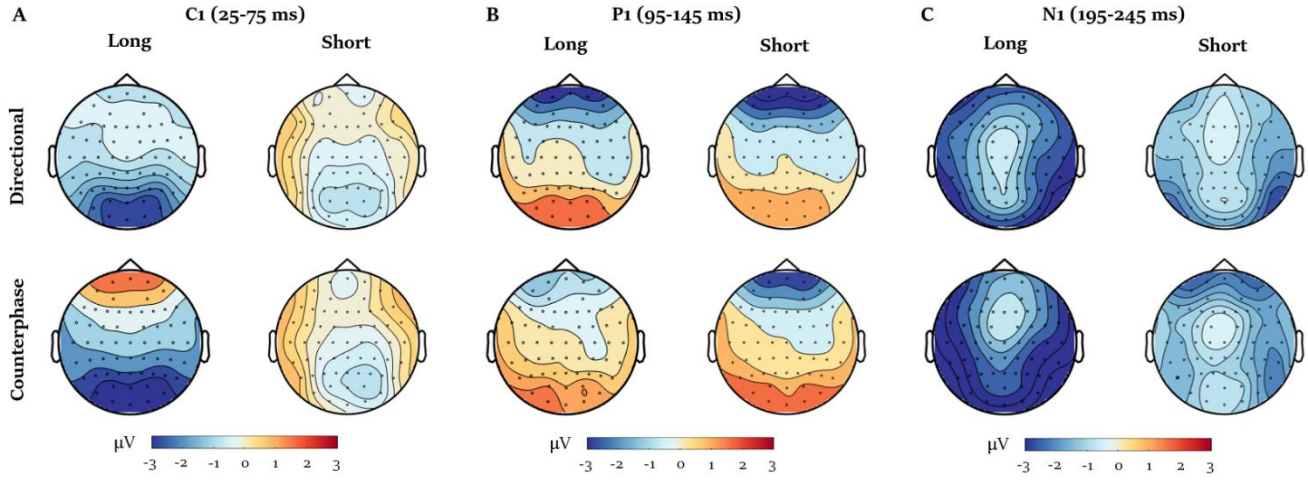

Supplementary Fig. S1. Voltage topographical maps of the grand averaged waveforms within the 50 ms time range of C1 (A), P1 (B) and N1 (C) components. The voltage topographical map of each adapter and duration condition is shown in separate rows and columns, respectively.

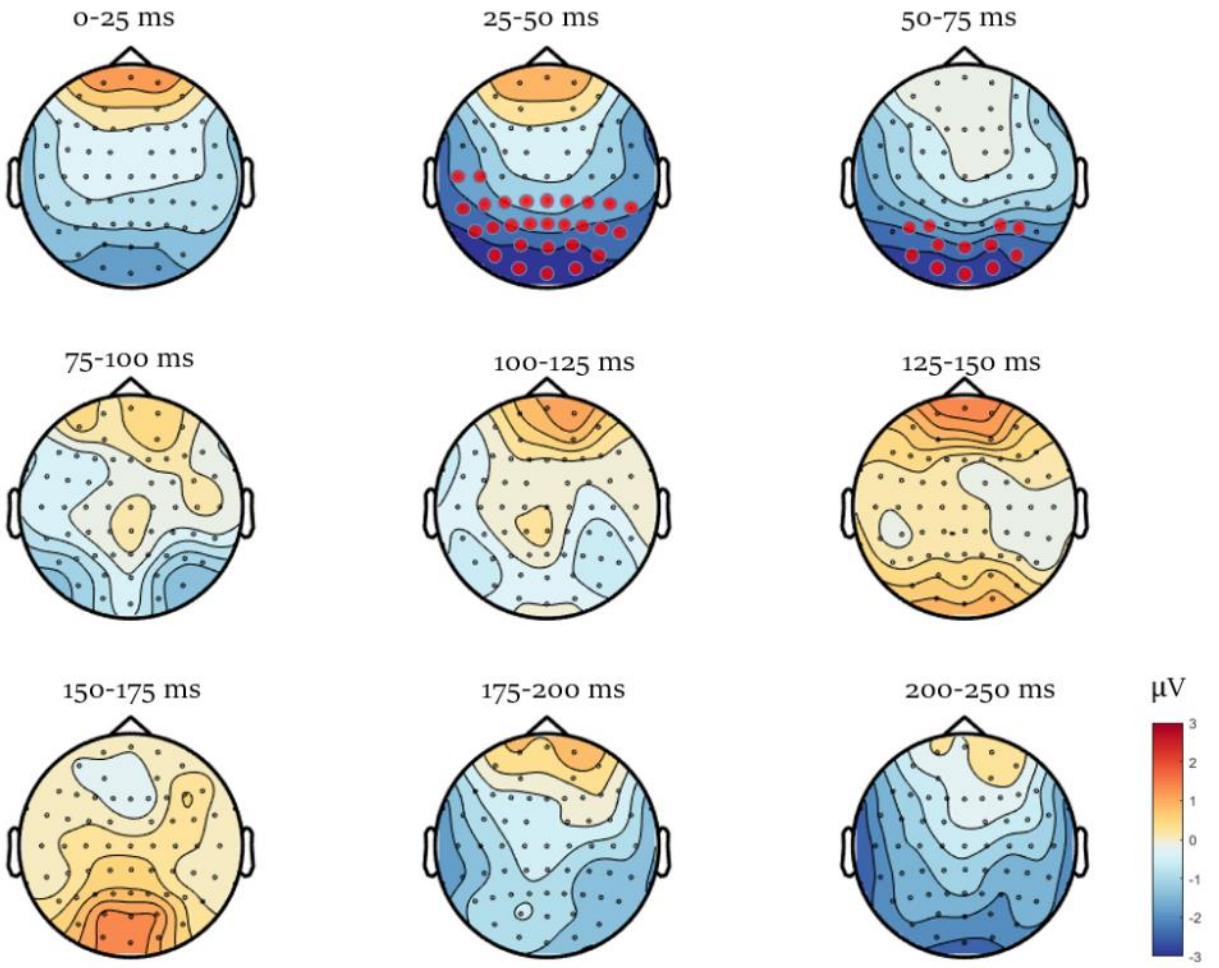

Supplementary Fig. S2. Results of the cluster-based permutation test comparing combined (i.e., averaged) ERPs of the short adaptation duration to those of long condition ($long_{combined}$ vs. $short_{combined}$). Voltage topographical maps of the grand averaged waveforms ($long_{combined}$ – $short_{combined}$) are shown within 25 ms time windows. The electrodes, which were part of the significant spatiotemporal cluster throughout each 25 ms time window, are marked by red filled circles on the topographical maps. These marked electrodes are *T7*, *C5*, *TP7*, *CP5*, *CP3*, *CP1*, *CPz*, *CP2*, *CP4*, *CP6*, *TP8*, *P7*, *P5*, *P3*, *P1*, *Pz*, *P2*, *P4*, *P6*, *P8*, *PO7*, *PO3*, *POz*, *PO4*, *PO8*, *O1*, *Oz*, *O2* for the 25-50 ms time window and *P5*, *P3*, *P4*, *P6*, *PO3*, *POz*, *PO4*, *O1*, *Oz*, *O2* for the 50-75 ms time window.

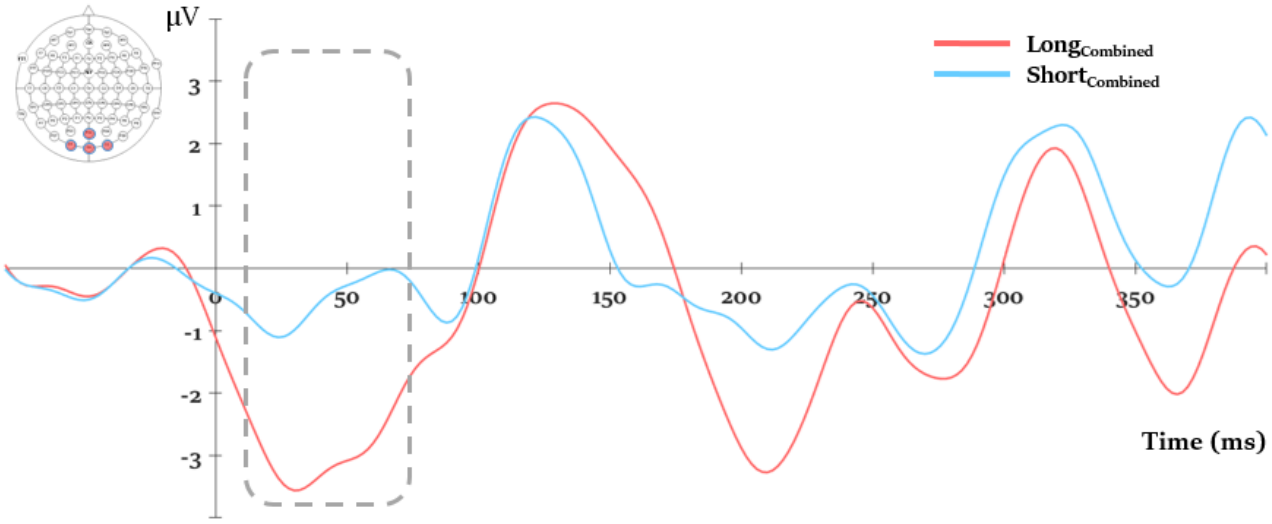

Supplementary Fig. S3. Averaged combined waveforms across all the electrodes (*POz*, *O1*, *Oz*, *O2*) located at the center of the significant spatiotemporal cluster in Fig. S2. The combined waveforms were time-locked to the onset of the test pattern and displayed in the range from -80 ms (i.e., the onset of the blank interval between adapter and test) to 400 ms. The identified time range based on the cluster-based permutation test is highlighted by a dashed rectangle.